PNAS
www.pnas.org

Supplementary Information for

Recruitment of pro-IL-1a to Mitochondrial Cardiolipin, via shared LC3 Binding Domain, Inihbits mitophagy, and Drives maximal NLRP3 Acitvation

Jargalsaikhan Dagvadorj, Karolina Mikulska-Ruminska, Gantsetseg Tumurkhuu, Rojo A. Ratsimandresey, Jessica Carriere, Allen M. Andres, Stefanie Marek Iannucci, Yang Song, Shuang Chen, Malcolm Lane, Andrea Dorfleutner, Roberta A. Gottlieb, Christian Stehlik[4], Suzanne Cassel, Fayyaz S. Sutterwala, Ivet Bahar, Timothy R. Crother and Moshe Arditi

Corresponding Authors: I.B., T.R.C., or M.A. (e-mail: bahar@pitt.edu, timothy.crother@cshs.org, or moshe.arditi@cshs.org)

This PDF file includes:

SI Methods
Figures S1 to S8
Tables S1 to S3
Legends for Movies S1 and S2
SI References

Other supplementary materials for this manuscript include the following:

Movies S1 to S2

SI Methods

Immunoprecipitation and protein-lipid overlay assay. HEK293 cells were transfected with pHIV-dTomato-mIL-1a-Flag or pHIV-dTomato-mIL-1a-RR-Flag using Lipofectamine 2000 transfection reagent (Invitrogen). Twenty-four hours after transfection, the cells were washed with 1X DPBS and lysed by sonication in NP-40 cell lysis buffer [50mM Tris pH 8.0, 150mM NaCl, 1% NP-40, 1mM PMSF, 1mM Na_3VO_4 and protease inhibitors cocktail (Roche)]. Total cell lysates were pre-cleared by centrifugation (14,000 rpm at 4°C for 5 min) and subjected to immunoprecipitation with 30 µL of 50% slurry anti-Flag M2 agarose affinity gel (Millipore) or isotype control (IgG, Santa Cruz Biotechnology) with Protein A/G agarose (Santa Cruz Biotechnology) for 16h at 4°C. The beads were washed extensively in NP-40 cell lysis buffer to remove unbound proteins. The beads were then blocked in 3% fatty acid-free BSA in TBS (25mM Tris, 150mM NaCl pH 7.2) for 15 min at 4°C followed by incubation with 10 µM sn-1-Fluorescein-labeled cardiolipin (Echelon Biosciences) for 30 min at room temperature in cardiolipin binding buffer (3% fatty acid-free BSA, 1mM $CaCl_2$ in TBS). The beads were washed extensively in TTBS (0.05% Tween-20 in TBS) to remove the unbound cardiolipin. The beads were placed into a black optical bottom 96-well plate and the FITC fluorescence intensity was measured at 29 points of each well using a Varioskan™ LUX multimode microplate reader (Thermofisher Scientific). Images were captured using an Echo Revolve fluorescent microscope (Echo). Finally, immunoprecipitated flag proteins were eluted by denaturing electrophoresis sample buffer and subjected to PAGE followed by immunoblotting and ECL detection.

LC3 Western Blot. After cell treatments, media was aspirated and cells were rinsed with PBS. Cells were then lifted from plates in PBS, transferred to a microfuge tube and spun down at 300xg for 5 mins. PBS was removed and 500µL mitochondrial isolation buffer (250mM Sucrose, 1mM EDTA, 10mM HEPES, pH 7.4) containing protease and phosphatase inhibitors (Roche) was added. Cells were then lysed mechanically by passing them through 27.5 gauge needle with a 1mL syringe 3 times. Nuclei and unbroken cells were eliminated by centrifuging homogenates at 1000xg, 4°C, for 5 mins. The resulting supernatant was then centrifuged further (7000xg, 4°C, 10 mins) to obtain the mitochondria-enriched heavy membrane fraction and separate the cytosol. The pellet was rinsed with a small volume of homogenization buffer (200µL) and re-spun down to eliminate the rinse buffer (7000xg, 4°C, 5 minutes). The mitochondria-enriched heavy membrane fraction was then resuspended in isolation RIPA buffer containing appropriate inhibitors. Samples were stored at -20°C until use.

Mitochondrial-enriched and cytosolic fractions and of samples were resolved using Bolt 4-12% Bis-Tris Plus gels and transferred onto nitrocellulose membranes. Blots were probed for LC3 (Cell Signaling). Immunoreactive bands were developed using Bio-Rad Clarity reagent and visualized with a ChemiDoc XRS system (Bio-Rad) followed by densitometry using NIH ImageJ software.

Cytokine assay. Cell culture supernatants were assayed using commercially available ELISA kits for murine IL-1β, IL-1α and TNF-α (eBioscience; San Diego, CA) according to the manufacturer's instructions. IL-18 level was determined by IL-18 ELISA kit (R and D).

Homology Modeling of Pro-IL1α structure. Pro-ILα consists of 271 residues, including an N-terminal segment of 112 residues which is cleaved upon maturation. Due to the absence of a structure for the intact pro-IL1α, we generated a structural model using available structural data for sequence homologs. First, we constructed a homology model for the S70-I109 region using Swiss-Model (1). To this end, we identified as templates the lipoprotein LptE (PDB (2) id: 5IVA, 20% sequence identity with respect to the fragment S70-I109) and a calcium-binding protein (2LGE, 40% sequence identity with respect to the same fragment) which shared similar secondary structure and contained the fragment of interest G78-L88 marked as signaling peptide (Fig. S3*A*). Second, the homology model and a crystal structure of mature IL1α (N121-A271, PDB id: 2KKI) were merged with the intervening sequence of 11 residues (K110-S120) using the AIDA package (3). The structurally unknown residues between the two fragments were computationally modeled to generate a unified structural model of 202 residues (Fig. S3*B*).

Equilibration of structural model and selection of stable conformer. Equilibration simulations were performed for human pro-IL1α (S70-A271) structural model using the NAMD (4) software package with the CHARMM27 force field (5) and explicit water models (TIP3P) (6). We adapted the following protocol: equilibration of water for 0.2 ns, 10,000 steps of energy minimization each step of size 2 fs, 0.35 ns of heating from 0 to 300 K, and 0.15 ns equilibration of the whole system before conducting a 200 ns all-atom molecular dynamics (MD) simulations to verify the equilibrium conformations of IL1α. We used 2 fs time step and a cutoff of 12 Å for non-bonded interactions. Langevin dynamics

and the Langevin piston algorithm were used to maintain isothermal and isobaric conditions at T = 300 K and P= 1 atm.

A total of 6 ensembles of structural models were identified upon clustering (principal component analysis, PCA) of the generated trajectory using the ProDy (7, 8) application programming interface (API) (Fig. S4). We used the mean shift algorithm (9) to distinguish the number of clusters, their distribution, and centers (see Fig. S4*A*). The structural model which exhibited the lowest average root-mean-square-deviation (RMSD) from all other members in a given cluster was further selected as a representative conformer for each cluster (Fig. *S4A*, *left, ribbon diagrams* color-coded after the clusters). The selected models were placed near a lipid bilayer which contained two types of lipid molecules: cardiolipin (CL) and 1,2-dioleoyl-sn-glycero-3-phosphocholine (DOPC) to examine the interactions between the protein and lipid molecules in MD simulations.

Molecular Dynamics (MD) simulations. We used CHARMM-GUI package (10) (11-13) for examining the stability and dynamics of the above selected 6 representative models. The simulation system contained over 70,000 atoms, including the lipid bilayer composed of DOPC and CL molecules (designated as PMCL2), water molecules, and Ca^{++} and Cl^{-} ions (Fig. S4*B*). The membrane was 80 Å long and wide, and contained 14 PMCL2 and 70 DOPC lipids. The protein was placed in the aqueous environment, with the closest distance of atom-atom approach from the membrane being 10 Å. We performed a series of simulations in the presence or absence of two posttranslational modifications: a phosphoserine at position 87 (pS87) and myristoylation of the lysines at position 82 and 83 (mK82, MK83), as indicated by UniProtKB (14) (accession number: P01583). These

modifications required the adoption of ten times longer system setup and minimization procedures compared to default parameters. One of the 6 structural models was observed to be stable and was selected for further studies: (a) 12 productive MD runs with pS87 and mK82-mK83 PTMs, and (b) 10 productive MD runs without phosphorylation of S87, but with mK82 and mK83. Each trajectory was 100 ns long. VMD (15) and ProDy (16) were used for visualizing and analyzing the trajectories.

Sequence alignment. Pairwise sequence alignment between Pro-IL-1α and LC3 was performed using ClustalX (17) and visualized with Jalview (18) using the LC3 sequence available in the PDB (PDB: 1UGM) and the S70-A271 fragment of Pro-IL1α used in MD studies.

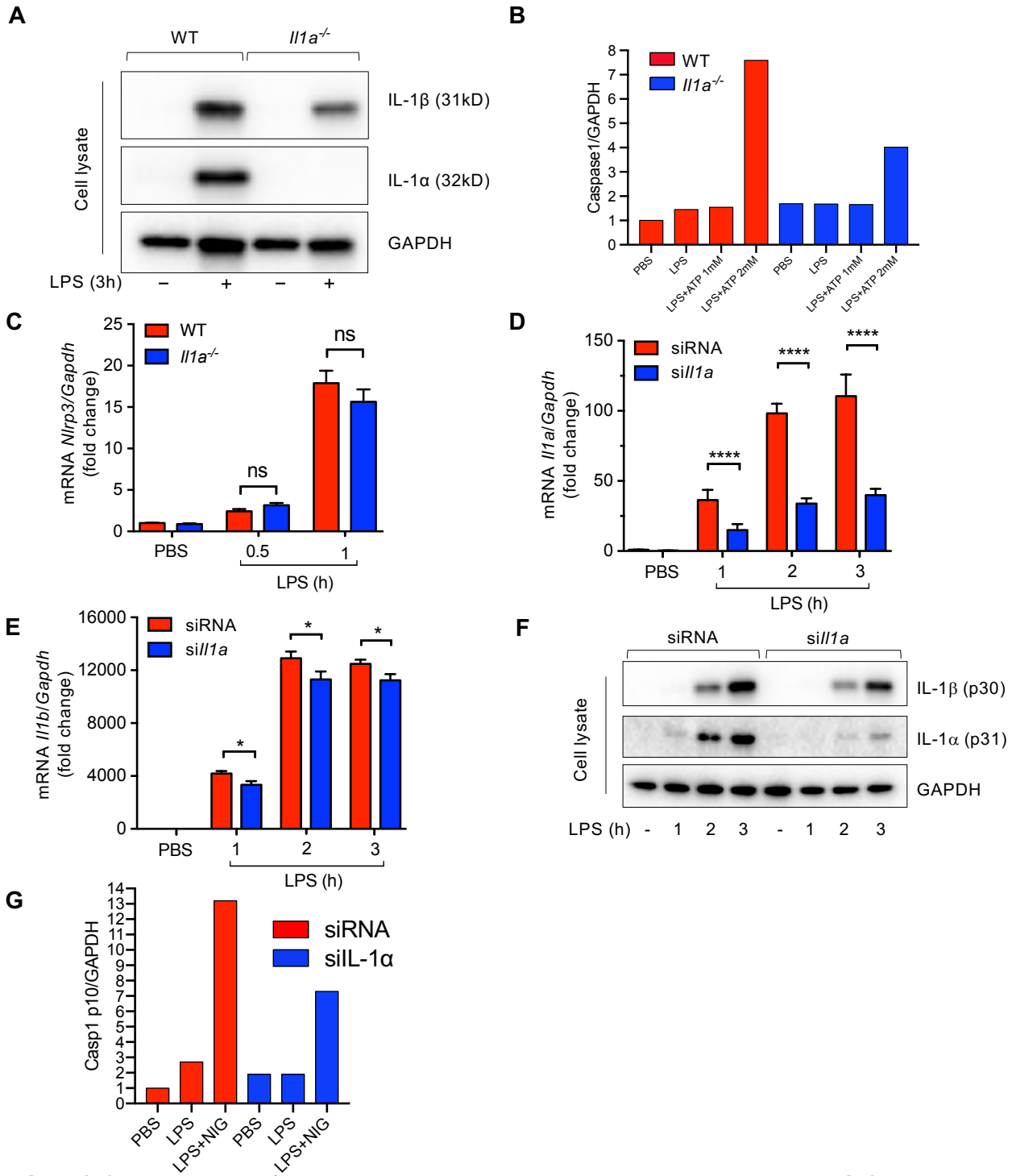

Figure S1. (A) Wt and I*l1a*$^{-/-}$ peritoneal macrophages were treated with LPS for 3 hr. IL-1α and IL-1β were assessed by immunoblot. (B) Densitometry analysis of cleaved Caspase-1 from Figure 1A. (C) *Nlrp3* mRNA expression was measured by quantitative RT-PCR in peritoneal macrophages following LPS stimulation. mRNA expression was normalized to the reference gene GAPDH. (D) *Il1a* mRNA expression was measured by quantitative RT-PCR in peritoneal macrophages transfected with siRNA or si*Il1a* for 48h and then stimulated with PBS or LPS for 3h. mRNA expression was normalized to the reference gene GAPDH. (E) *Il1b* mRNA expression was measured by quantitative RT-PCR in peritoneal macrophages transfected with siRNA or si*Il1a* for 48h and then stimulated with PBS or LPS for 3h. mRNA expression was normalized to the reference gene GAPDH. (F) WT peritoneal macrophages were transfected with siRNA or si*Il1a* for 48h and stimulated with PBS or LPS for 3h. Immunoblotting analysis for IL-1β and IL-1α in cell lysate. (G) Densitometry analysis of cleaved Caspase-1 from Figure 1H. Results are representative of 3 independent experiments. All data represent mean ± SD; (Student's t-test), *p<0.05, ***p<0.001.

Membrane potential TMRM 200nM

WT ***Il1a*$^{-/-}$**

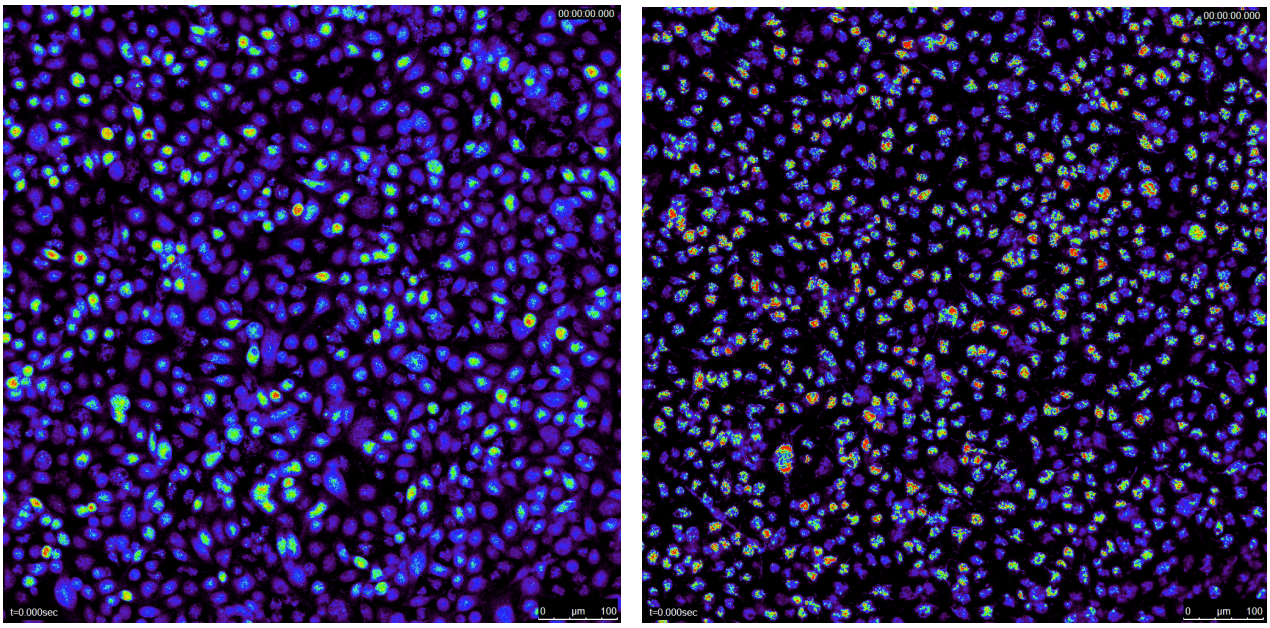

LPS (3h) +ATP (2mM)

Movie S1 and S2. WT (S1) and *Il1a*$^{-/-}$ (S2) peritoneal macrophages were treated with LPS and ATP and stained with TMRM to observe mitochondrial membrane potential changes.

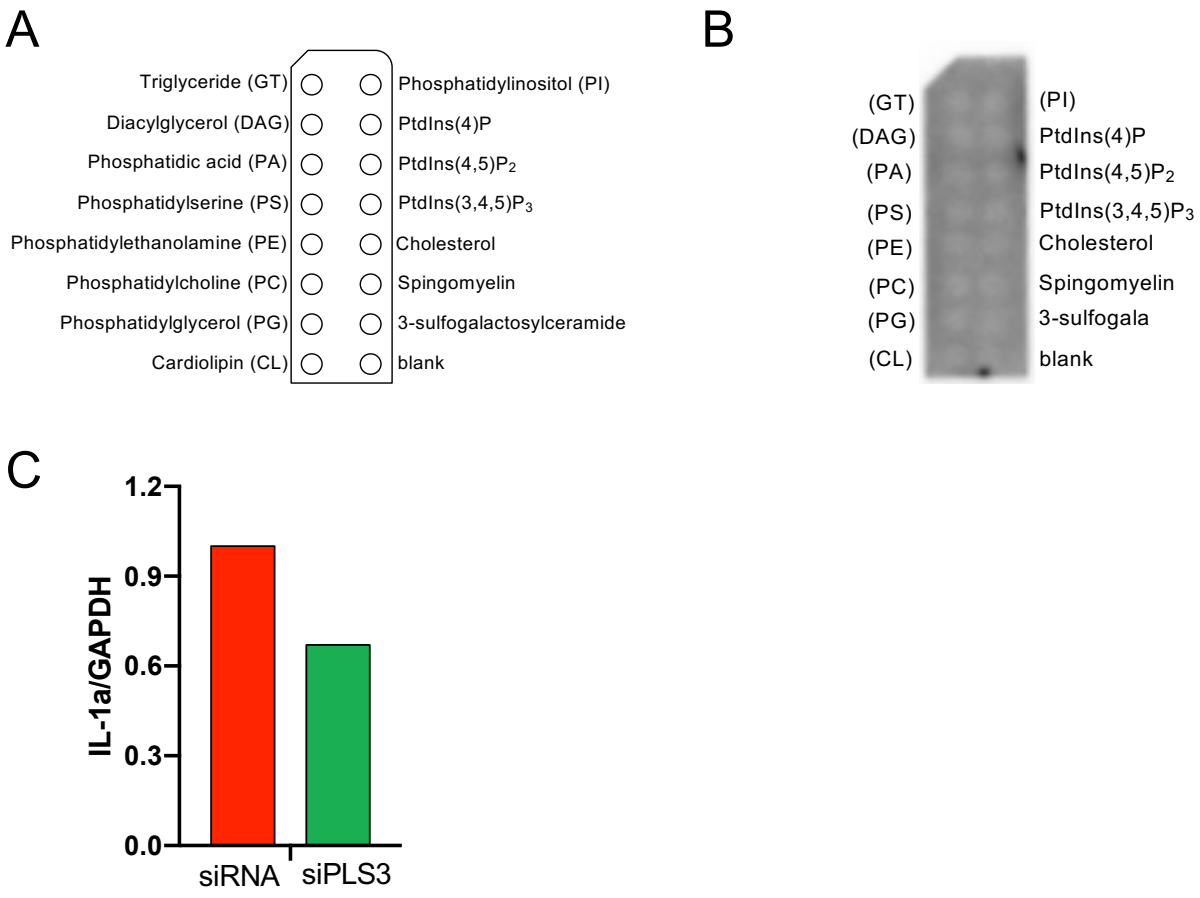

Figure S2. (A) Layout of lipid strip samples. (B) Lipid Strip probes with cell lysates from unstimulated WT peritoneal macrophages. (C) Densitometric analysis of IL-1α present in mitochondrial fraction from Figure 2F.

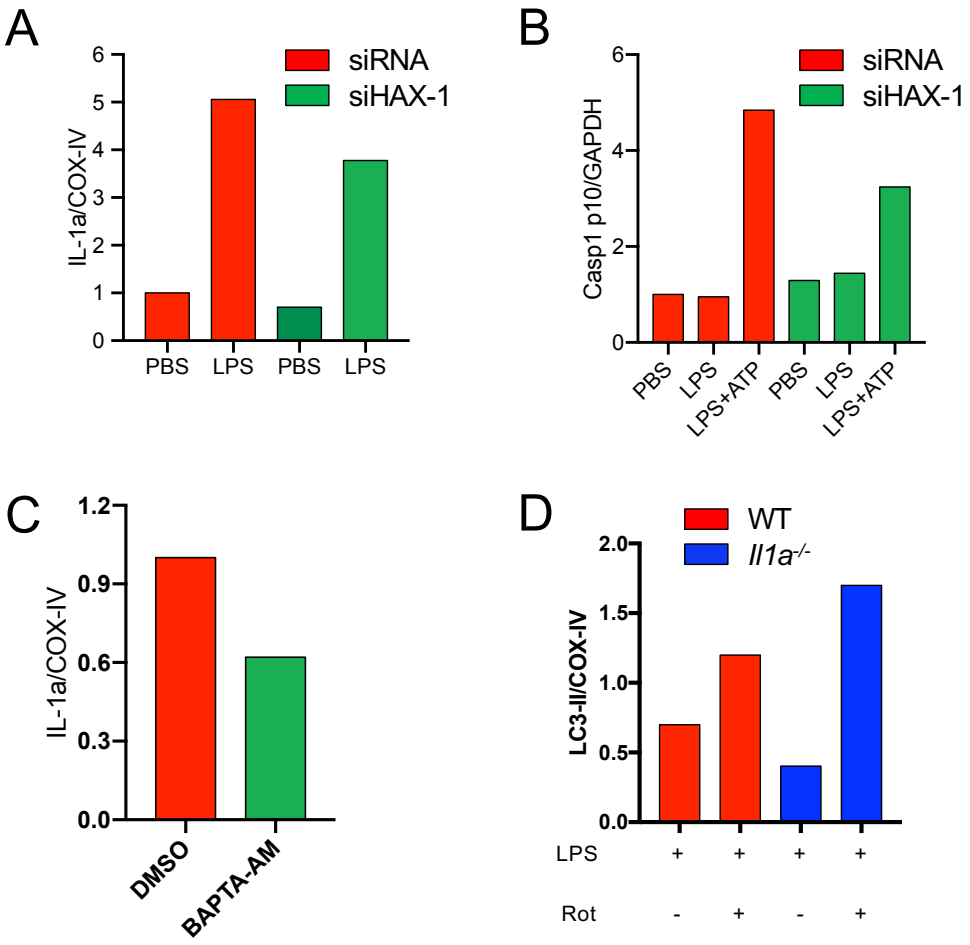

Figure S3. (A) Densitometric analysis of IL-1α present in mitochondrial fraction from Figure 3A. (B) Densitometric analysis of cleaved Caspase-1 present in cytosolic fraction from Figure 3B. (C) Densitometric analysis of IL-1α present in mitochondrial fraction from Figure 3E. (D) Densitometric analysis of LC3-II present in mitochondrial fraction from Figure 4B normalized to COX-IV.

A

Homology modeling (Swiss Model)

Metal binding protein

Name	Title	Coverage	Identity	Method
2lge.1.A	Uncharacterized protein		40.74	NMR
2lg7.1.A	Uncharacterized protein		40.74	NMR

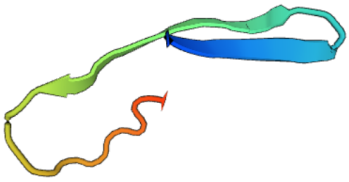

target peptide

Lipoprotein LptE

2n8x.1.A	LPS-assembly lipoprotein LptE	19.51	NMR	
5tse.1.A	LPS-assembly lipoprotein LptE	14.29	X-ray, 2.3Å	
5tse.2.A	LPS-assembly lipoprotein LptE	14.29	X-ray, 2.3Å	
5tse.3.A	LPS-assembly lipoprotein LptE	14.29	X-ray, 2.3Å	
5ixm.4.B	LPS-assembly lipoprotein LptE	17.50	X-ray, 2.7Å	
5ixm.3.B	LPS-assembly lipoprotein LptE	17.50	X-ray, 2.7Å	
5ixm.2.B	LPS-assembly lipoprotein LptE	17.50	X-ray, 2.7Å	
5ixm.1.B	LPS-assembly lipoprotein LptE	17.50	X-ray, 2.7Å	
5iva.1.B	LPS-assembly lipoprotein LptE	20.00	X-ray, 3.0Å	
4rhb.1.B	LPS-assembly lipoprotein LptE	20.00	X-ray, 3.4Å	

target peptide

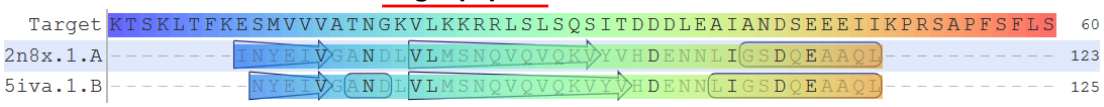

B

Construction of pro-IL-1α (AIDA)

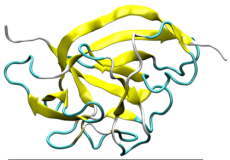

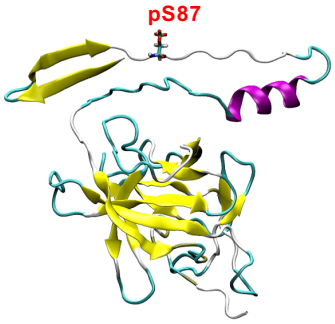

S70-I109 + K110-S120 + N121-A271 =

IL-1a pro-piece with target peptide | Linker | Mature IL-1a PDB code: 2kkl | proIL-1α (S70-A271)

Sequence used for predictions:

>sp|P01583|IL1A_HUMAN Interleukin-1 alpha OS=Homo sapiens GN=IL1A PE=1 SV=1

MAKVPDMFEDLKNCYSENEEDSSSIDHLSLNQKSFYHVSYGPLHEGCMDQSVSLSISETSKTSKLTFKESMVVVATNGKVLKKRRLSLSQSI
TDDDLEAIANDSEEEIIKPRSAPFSFLSNVKYNFMRIIKYEFILNDALNQSIIRANDQYLTAAALHNLDEAVKFDMGAYKSSKDDAKITVIL
RISKTQLYVTAQDEDQPVLLKEMPEIPKTITGSETNLLFFWETHGTKNYFTSVAHPNLFIATKQDYWVCLAGGPPSITDFQILENQA

Molecular Dynamics (MD) simulation

Figure S4. Construction of pro-IL1α model (S70-A271). (A) Homology modeling of S70-I109 fragment based on a metal-binding protein (PDB: 2lge, 40% sequence identity with respect to pro-IL-1α) and lipoprotein LptE (5iva, 20% sequence identity). We identified two templates using Swiss-Model server. The alignments of the selected templates and target sequence are shown together with the corresponding secondary structures and 3D models. The analysis also yielded a few other lipoproteins with lower sequence identity and coverage. (B) Construction of S70-A271 portion of pro-IL1α by stitching together three fragments: (1) Homology model for S70-I109 which contains the signal peptide G78-L88, obtained from Swiss-Model, (2) the K110-S120 fragment not resolved structurally, and (3) the mature IL1α structure available in the PDB as 2KKI: N121-A271. As a last step 200 ns MD simulation with explicit solvent was performed for generating a stable conformer.

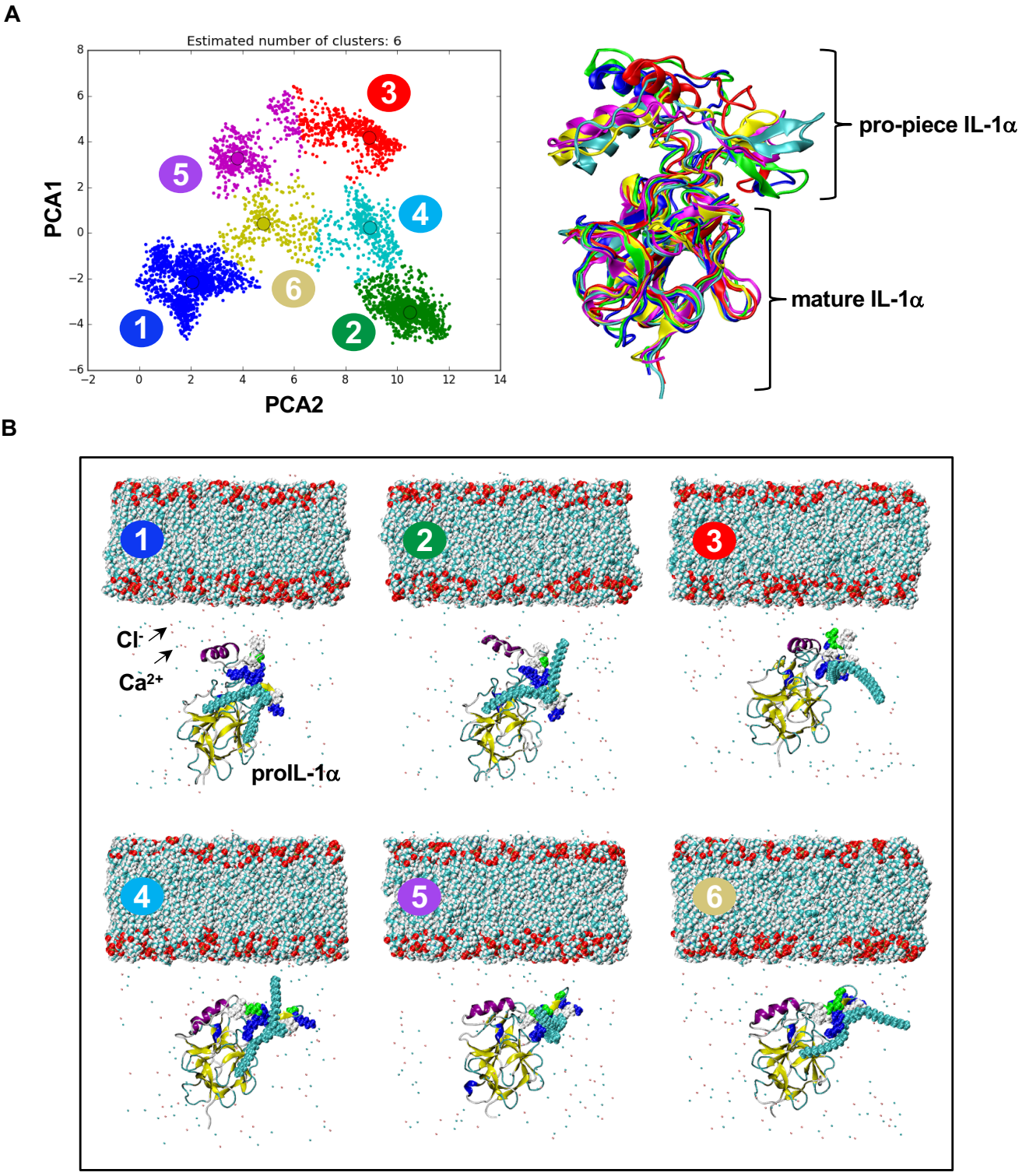

Figure S5. Structural models identified by PCA of 200 ns MD trajectories generated for pro-IL1α fragment S70-A271. (A) Distribution of pro-IL1α conformations into six clusters: 1-*blue*, 2-*green*, 3-*red*, 4-*cyan*, 5-*magenta*, 6-*yellow*. *Right panel* shows the structural alignment of the 6 conformers representative of each cluster. Structural models are colored by the corresponding cluster. (B) Six equilibrium conformers of pro-IL1α placed near a lipid bilayer that contains CL and DOPC molecules. The signal peptide in each case is displayed in *balls representation* (color guide: *cyan* – mK82-83, *blue* – charged residues from G78-L88). Small points represent Ca^{2+} and Cl^{-} ions.

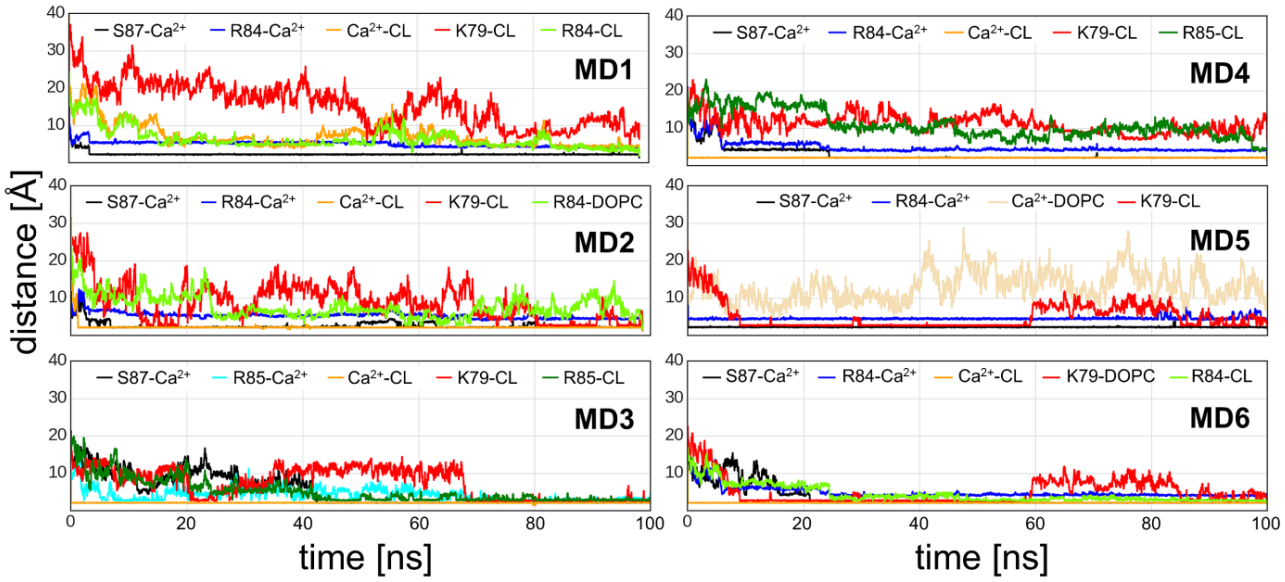

Figure S6. Evolution in the distance for 6 MD runs of Type I interactions of pro-IL1α, Ca^{2+} ion and the membrane lipids (CL and DOPC).

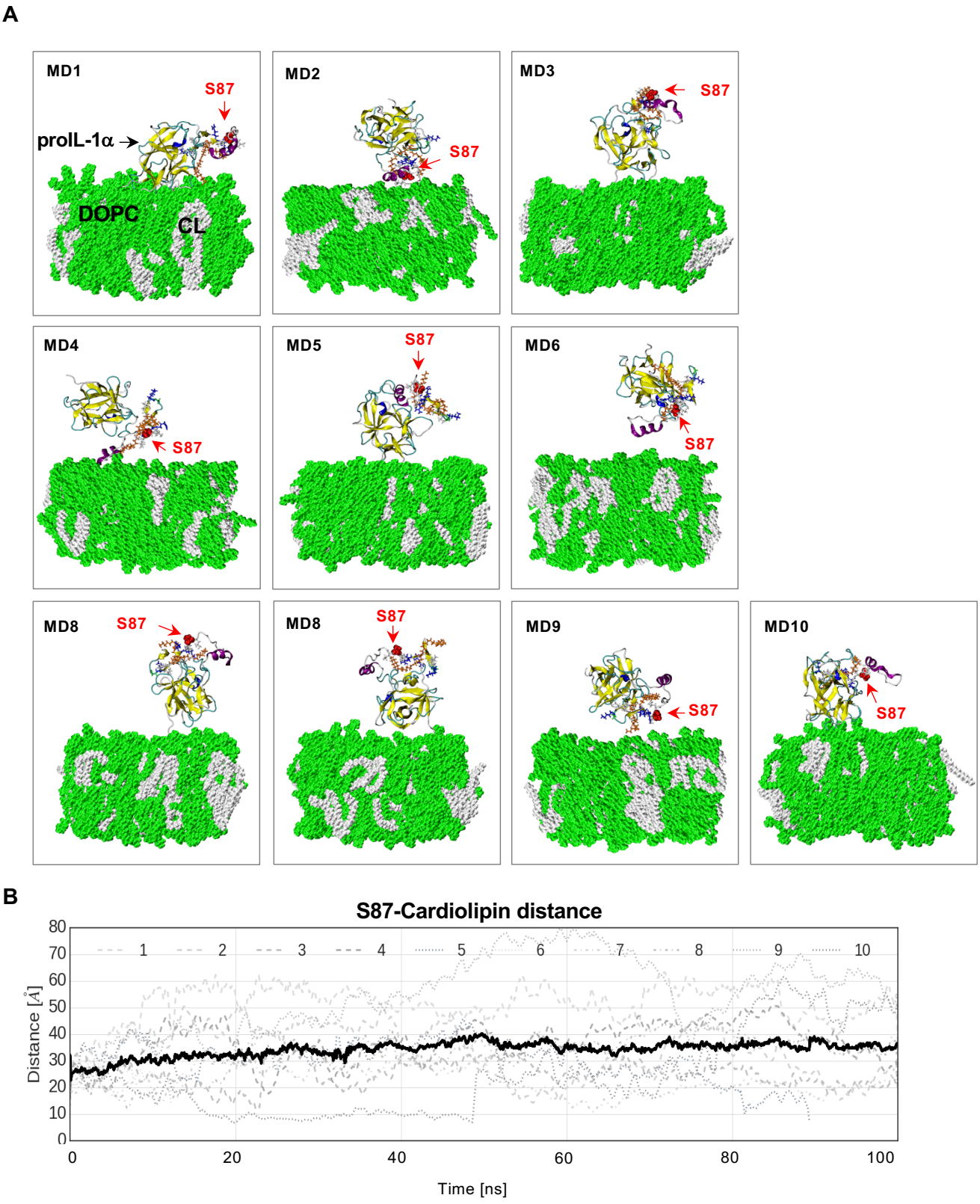

Figure S7. Lack of interaction between Pro-IL1α S87 and CL molecules in the absence of S87 phosphorylation. (A) Snapshots from 10 independent runs illustrate the lack of a stable interaction between pro-IL1α with DOPC-CL-bilayer. Color guide: DOPC: *green*, CL: *white*, S87 from pro-IL1α: *red spheres*, mK82-K83 from pro-IL1α: *orange*. *Red arrows* point the position of signal peptide residues (G78-L88). (B) Time evolution of the distance between S87 and the closest CL for each of 10 MD runs (*grey dotted lines*). Average curve of all 10 runs maintains the distance of 25-40 Å, shown in *black*.

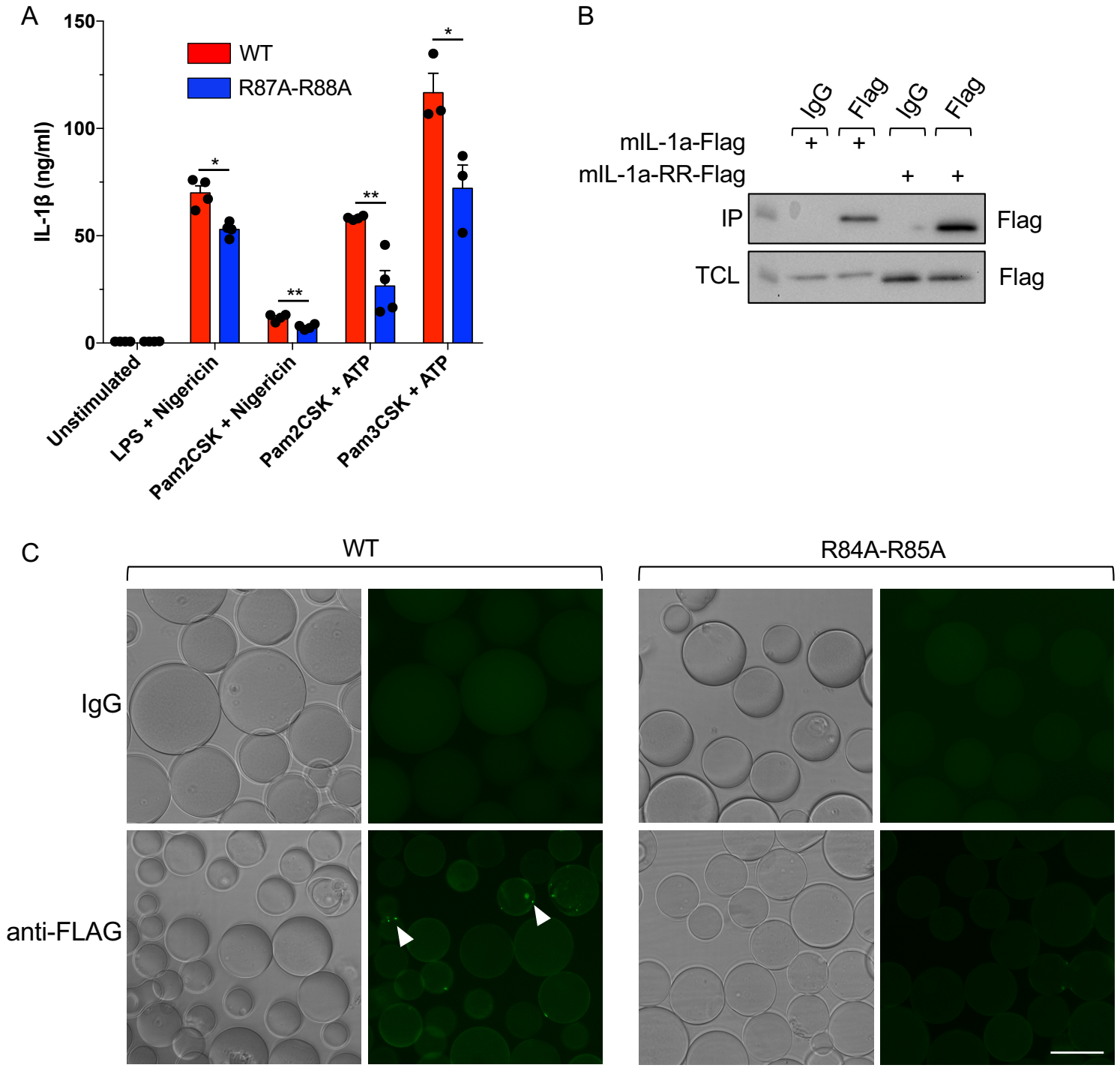

Figure S8. Mutated pro-IL-1α reduces IL-1β secretion and CL binding. (A) *Il1a*$^{-/-}$ bone marrow derived macrophages were reconstituted with WT or R84A-R85A mouse *Il1a* and primed and stimulated with indicated reagents. IL-1β secretion measured by ELISA. (B and C) HEK293 cells were transfected with mIL-1a-WT-Flag or mIL-1a-RR-Flag. Anti-FLAG beads were used to immunoprecipitate the FLAG-proteins. Western blot showing WT and R87A-R88A IP (B). FITC labeled CL binding to pro-IL-1α-FLAG beads shown by fluorescent microscopy (C). Student's t-test was used to analyze the data. *p<0.05, **p<0.01.

Table S1. List of motifs variants checked in SwissProt database

Motif	# proteins	# type of proteins	# human proteins
KxxKxRRxSxxQ	20	6	2
KxxKxRR-SxxQ	7	6	1
KxxKxRRxS	159	99	18
KxxKxRR-S	191	92	13
KxxKKRRxS	40	20	5
KxxKKRR-S	7	7	0

Table S2. Selected list of proteins characterized by cardiolipin binding site motif present in pro-IL1α and LC3. Listed proteins contain information about UniProtID, pathway (based on Reactome information) and/or PDB codes which contain characteristic motif.

Motif: KxxKxRRxS					
Name	**Protein full name**	**UniProtID**	**Pathway Name**	**ReactomeID**	**PDB code**
ABLM3_HUMAN	Actin-binding LIM protein 3	O94929	DCC mediated attractive signaling	R-HSA-418885	-
ANAPT_NEOFI	Indole diterpene prenyltransferase anaPT	A1DN10	-	-	4LD7
ANM5_HUMAN	Protein arginine N-methyltransferase 5	O14744	snRNP Assembly, RMTs methylate histone arginines, Regulation of TP53 Activity through Methylation	R-HSA-191859, R-HSA-3214858, R-HSA-6804760	4GQB, 4X60, 4X61, 4X63, 5C9Z, 5EMJ, 5EMK, 5EML, 5EMM, 5FA5, 6CKC, 6K1S
ARI4B_HUMAN	AT-rich interactive domain-containing protein 4B	Q4LE39	HDACs deacetylate histones, NoRC negatively regulates rRNA expression	R-HSA-3214815, R-HSA-427413	-
CP51_SCHPO	Lanosterol 14-alpha demethylase erg11	Q09736	Cholesterol biosynthesis, Endogenous sterols	R-SPO-191273, R-SPO-211976	-
CWC22_DROME	Pre-mRNA-splicing factor CWC22 homolog	Q9VJ87	mRNA Splicing - Major Pathway	R-DME-72163	-
DAPK3_HUMAN†	Death-associated protein kinase 3	O43293	Ligand-independent caspase activation via DCC	R-HSA-418889	1YRP, 2J90, 3BHY, 3BQR, 5A6N, 5A6O, 5VJA
GCOB_AMYS7	Aromatic O-demethylase	P0DPQ8	-	-	5OGX
GEM1_YEAST	Mitochondrial Rho GTPase 1	P39722	Rho GTPase cycle	R-SCE-194840	-

GRK7A_DANRE†	Rhodopsin kinase 1	Q49HM9	Inactivation, recovery and regulation of the phototransduction cascade	R-DRE-2514859	-
GRK7B_DANRE†	Rhodopsin kinase 2	Q1XHL7	Inactivation, recovery and regulation of the phototransduction cascade	R-DRE-2514859	-
GSH1_CAEEL	Glutamate--cysteine ligase	Q20117	Glutathione synthesis and recycling	R-CEL-174403	-
HFA6B_ORYSJ	Heat stress transcription factor A-6a	Q657C0	Regulation of HSF1-mediated heat shock response, HSF1 activation, Attenuation phase, HSF1-dependent transactivation	R-OSA-3371453, R-OSA-3371511, R-OSA-3371568, R-OSA-3371571	-
HFD1_YEAST	Fatty aldehyde dehydrogenase HFD1	Q04458	Sphingolipid de novo biosynthesis, Phase I - Functionalization of compounds, Alpha-oxidation of phytanate, Neutrophil degranulation	R-SCE-1660661, R-SCE-211945, R-SCE-389599, R-SCE-6798695	-
IL1A_BOVIN*†	Interleukin-1 alpha	P08831	Interleukin-1 processing, Interleukin-1 signaling	R-BTA-448706, R-BTA-9020702	-
IL1A_HUMAN*†	Interleukin-1 alpha	P01583	Senescence-Associated Secretory Phenotype (SASP), Interleukin-1 processing, Interleukin-10 signaling, Interleukin-4 and 13 signaling, Interleukin-1 signaling	R-HSA-2559582, R-HSA-448706, R-HSA-6783783, R-HSA-6785807, R-HSA-9020702	-
IL1A_MOUSE*†	Interleukin-1 alpha	P01582	Interleukin-1 processing, Interleukin-1 signaling	R-MMU-448706, R-MMU-9020702	-
IL1A_PIG*†	Interleukin-1 alpha	P18430	Interleukin-1 processing, Interleukin-1 signaling	R-SSC-448706, R-SSC-9020702	-
JMJ14_ARATH	Probable lysine-specific demethylase JMJ14	Q8GUI6	HDMs demethylate histones	R-ATH-3214842	-
KCR1_ARATH	Very-long-chain 3-oxoacyl-CoA reductase 1	Q8L9C4	Androgen biosynthesis, Synthesis of very long-chain fatty acyl-CoAs	R-ATH-193048, R-ATH-75876	-
LPIN1_HUMAN	Phosphatidate phosphatase LPIN1	Q14693	Synthesis of PC, Synthesis of PE, Depolymerisation of the Nuclear Lamin, Triglyceride biosynthesis	R-HSA-1483191, R-HSA-1483213, R-HSA-4419969, R-HSA-75109	-
NIPLB_DANRE	Nipped-B-like protein B	F1QBY1	Cohesin Loading onto Chromatin	R-DRE-2470946	-
PERM_HUMAN*	Myeloperoxidase	P05164	Neutrophil degranulation	R-HSA-6798695	-
PO6F1_HUMAN	POU domain, class 6, transcription factor 1	Q14863	-	-	3D1N
RBBP6_HUMAN	E3 ubiquitin-protein ligase RBBP6	Q7Z6E9	Antigen processing: Ubiquitination & Proteasome degradation	R-HSA-983168	-
RBBP6_MOUSE	E3 ubiquitin-protein ligase RBBP6	P97868	Antigen processing: Ubiquitination & Proteasome degradation	R-MMU-983168	-
REV3L_HUMAN	DNA polymerase zeta catalytic subunit	O60673	Translesion synthesis by REV1, Translesion synthesis by POLK, Translesion synthesis by POLI	R-HSA-110312, R-HSA-5655862, R-HSA-5656121	-
RN19A_HUMAN†	E3 ubiquitin-protein ligase RNF19A	Q9NV58	Antigen processing: Ubiquitination & Proteasome degradation	R-HSA-983168	-
RN19A_MOUSE	E3 ubiquitin-protein ligase RNF19A	P50636	Antigen processing: Ubiquitination & Proteasome degradation	R-MMU-983168	-
RN19A_PIG†	E3 ubiquitin-protein ligase RNF19A	Q2VJ60	Antigen processing: Ubiquitination & Proteasome degradation	R-SSC-983168	-

RPOL_BPT7	T7 RNA polymerase	P00573	-	-	1ARO, 1CEZ, 1H38, 1MSW, 1QLN, 1S0V, 1S76, 1S77, 2PI4, 2PI5, 3E2E, 3E3J, 4RNP
SSRP1_HUMAN†	FACT complex subunit SSRP1	Q08945	Formation of RNA Pol II elongation complex, Formation of HIV elongation complex in the absence of HIV Tat, Formation of HIV-1 elongation complex containing HIV-1 Tat, Pausing and recovery of Tat-mediated HIV elongation, Tat-mediated HIV elongation arrest and recovery, Tat-mediated elongation of the HIV-1 transcript, HIV elongation arrest and recovery, Pausing and recovery of HIV elongation, RNA Polymerase II Pre-transcription Events, TP53 Regulates Transcription of DNA Repair Genes, Regulation of TP53 Activity through Phosphorylation, RNA Polymerase II Transcription Elongation	R-HSA-112382, R-HSA-167152, R-HSA-167200, R-HSA-167238, R-HSA-167243, R-HSA-167246, R-HSA-167287, R-HSA-167290, R-HSA-674695, R-HSA-6796648, R-HSA-6804756, R-HSA-75955	-
SSRP1_MOUSE†	FACT complex subunit SSRP1	Q08943	Formation of RNA Pol II elongation complex, RNA Polymerase II Pre-transcription Events, TP53 Regulates Transcription of DNA Repair Genes, Regulation of TP53 Activity through Phosphorylation, RNA Polymerase II Transcription Elongation	R-MMU-112382, R-MMU-674695, R-MMU-6796648, R-MMU-6804756, R-MMU-75955	-
SSRP1_RAT†	FACT complex subunit SSRP1	Q04931	Formation of RNA Pol II elongation complex, RNA Polymerase II Pre-transcription Events, TP53 Regulates Transcription of DNA Repair Genes, Regulation of TP53 Activity through Phosphorylation, RNA Polymerase II Transcription Elongation	R-RNO-112382, R-RNO-674695, R-RNO-6796648, R-RNO-6804756, R-RNO-75955	-
TRPM5_HUMAN	Transient receptor potential cation channel subfamily M member 5	Q9NZQ8	TRP channels	R-HSA-3295583	-
TTF1_HUMAN†	Transcription termination factor 1	Q15361	ERCC6 (CSB) and EHMT2 (G9a) positively regulate rRNA expression, NoRC negatively regulates rRNA expression, Surfactant metabolism, Defective pro-SFTPB causes pulmonary surfactant metabolism dysfunction 1 (SMDP1) and respiratory distress syndrome (RDS), RNA Polymerase I Transcription Initiation, RNA Polymerase I Transcription	R-HSA-427389, R-HSA-427413, R-HSA-5683826, R-HSA-5688031, R-HSA-73762, R-HSA-73863	-

			Termination		
Motif: KxxKxRRS					
Name	**Protein name**	**UniProtID**	**Pathway Name**	**ReactomeID**	**PDB code**
AB12C_ARATH	ABC transporter C family member 12	Q9C8H0	Platelet degranulation, Hyaluronan biosynthesis and export, ABC-family proteins mediated transport, Ub-specific processing proteases, Cargo recognition for clathrin-mediated endocytosis	R-ATH-114608, R-ATH-2142850, R-ATH-382556, R-ATH-5689880, R-ATH-8856825	-
BARX1_HUMAN	Homeobox protein BarH-like 1	Q9HBU1	-	-	2DMT
CP51_SCHPO	Lanosterol 14-alpha demethylase erg11	Q09736	Cholesterol biosynthesis, Endogenous sterols	R-SPO-191273, R-SPO-211976	-
E41L5_BOVIN	Band 4.1-like protein 5	Q58CU2	Neurexins and neuroligins	R-BTA-6794361	-
E41L5_HUMAN	Band 4.1-like protein 5	Q9HCM4	Neurexins and neuroligins	R-HSA-6794361	-
E41L5_MOUSE	Band 4.1-like protein 5	Q8BGS1	Neurexins and neuroligins	R-MMU-6794361	-
E41L5_RAT	Band 4.1-like protein 5	Q5FVG2	Neurexins and neuroligins	R-RNO-6794361	-
GFLB_DICDI	Ras guanine nucleotide exchange factor glfB	Q54L90	p38MAPK events, NRAGE signals death through JNK, Rho GTPase cycle, G alpha (12/13) signalling events, RAF/MAP kinase cascade	R-DDI-171007 R-DDI-193648 R-DDI-194840 R-DDI-416482 R-DDI-5673001	-
GTR3_DROME	Glucose transporter type 3	P53403	Cellular hexose transport, Cargo recognition for clathrin-mediated endocytosis, Clathrin-mediated endocytosis	R-DME-189200, R-DME-8856825, R-DME-8856828	-
ING2_HUMAN	Inhibitor of growth protein 2	Q9H160	PI5P Regulates TP53 Acetylation	R-HSA-6811555	-
MLP3B_MOUSE*	Microtubule-associated proteins 1A/1B light chain 3B	Q9CQV6	Macroautophagy, Pink/Parkin Mediated Mitophagy, TBC/RABGAPs, Receptor Mediated Mitophagy	R-MMU-1632852, R-MMU-5205685, R-MMU-8854214, R-MMU-8934903	5WRD, 5YIQ, 5YIS
MLP3B_RAT*	Microtubule-associated proteins 1A/1B light chain 3B	Q62625	-	-	1UGM, 2K6Q, 2Z0D, 2Z0E, 2ZZP
NIPLB_DANRE	Nipped-B-like protein B	F1QBY1	Cohesin Loading onto Chromatin	R-DRE-2470946	-

OSTP_PIG*	Osteopontin	P14287	Degradation of the extracellular matrix, Signaling by PDGF, Integrin cell surface interactions, Regulation of Insulin-like Growth Factor (IGF) transport and uptake by Insulin-like Growth Factor Binding Proteins (IGFBPs), Post-translational protein phosphorylation	R-SSC-1474228, R-SSC-186797, R-SSC-216083, R-SSC-381426, R-SSC-8957275	-
RHG20_HUMAN	Rho GTPase-activating protein 20	Q9P2F6	Rho GTPase cycle	R-HSA-194840	-
RHG20_MOUSE	Rho GTPase-activating protein 20	Q6IFT4	Rho GTPase cycle	R-MMU-194840	-
RHG20_RAT	Rho GTPase-activating protein 20	Q6REY9	Rho GTPase cycle	R-RNO-194840	-
RUSD4_HUMAN	Mitochondrial RNA pseudouridine synthase RPUSD4	Q96CM3	-	-	5UBA
UBD_HUMAN	Ubiquitin D	O15205	Neddylation	R-HSA-8951664	2MBE, 6GF1
XPB2_ARATH	General transcription and DNA repair factor IIH helicase subunit XPB2	Q9FUG4	Formation of the Early Elongation Complex, Formation of Incision Complex in GG-NER, Dual Incision in GG-NER, RNA Polymerase II Pre-transcription Events, Formation of TC-NER Pre-Incision Complex, Dual incision in TC-NER, Gap-filling DNA repair synthesis and ligation in TC-NER, TP53 Regulates Transcription of DNA Repair Genes, mRNA Capping, RNA Polymerase II Promoter Escape, RNA Polymerase II Transcription Pre-Initiation And Promoter Opening, RNA Polymerase II Transcription Initiation, RNA Polymerase II Transcription Initiation And Promoter Clearance, RNA Pol II CTD phosphorylation and interaction with CE	R-ATH-113418, R-ATH-5696395, R-ATH-5696400, R-ATH-674695, R-ATH-6781823, R-ATH-6782135, R-ATH-6782210, R-ATH-6796648, R-ATH-72086, R-ATH-73776, R-ATH-73779, R-ATH-75953, R-ATH-76042, R-ATH-77075	-
ZN607_HUMAN	Zinc finger protein 607	Q96SK3	Generic Transcription Pathway	R-HSA-212436	-

* Present in KxxKxRRxSxxQ or KxxKxRR-SxxQ motif.

† Present in KxxK**K**RRxS

Table S3. Key Resources

REAGENT or RESOURCE	SOURCE	IDENTIFIER
Antibodies		
Anti-IL-1a	R&D system	Cat # AF-400-NA
Anti-Nlrp3	R&D system	Cat # MAB7578
Anti-Caspase1 p12/p10	Abcam	Cat # 179515
Anti-COX IV	Cell Signaling	Cat # 4844
Anti-GAPDH (D16H11)	Cell Signaling	Cat # 5174
Anti-Cytochrome c (D18C7) Rabbit mAb	Cell Signaling	Cat # 11940S
Anti-LC3b DyLight 650	Thermofisher Scientific	Cat # PA5-22937
Anti-His Tag, pAb, Rabbit	GenScript	Cat # A00174-40
Anti-PLSCR3	Abcam	Cat # ab137128
Anti-LC3	Cell Signaling	Cat # 4108
Anti-Pink1	Abcam	Cat# ab23707
Anti-GAPDH	Santa Cruz Biotech	Cat# sc-137139
Anti-Flag M2, mAb, Mouse	Sigma-Aldrich	Cat # F3165-1MG
Normal mouse IgG	Santa Cruz Biotechnology	Cat # sc-2025
Goat anti-mouse IgG-HRP	Santa Cruz Biotechnology	sc-2005
Bacterial and Virus Strains		
Biological Samples		
Mouse peritoneal macrophages		
HEK293 cell line		
Lenti-X 293T	Takara/Clontech	Cat# 632180
MCL cell line		
L929 cells supernatant	ATCC	CCL-1
Chemicals, Peptides, and Recombinant Proteins		
IL1A (Human) Recombinant Protein (P01)	Abnova	Cat # H00003552-P01
Membrane Lipid Strips	Echelon Biosciences	Cat # P-6002

ATP	Thermofisher Scientific	Cat # R0441
Pam2CSK4	Invivogen	Cat # tlrl-pm2s-1
LPS	Sigma Aldrich	Cat # L2630
sn-1-Fluorescein-labeled cardiolipin	Echelon Biosciences	Cat # L-C16F
NIGERICIN	Enzo Life Sciences	BML-CA421-0005
ANTI-FLAG® M2 Affinity Gel	Millipore	Cat # A2220-1ML
Protein A/G agarose	Santa Cruz Biotechnology)	Cat # sc-2003
Critical Commercial Assays		
Mitochondria Isolation Kit	Abcam	Cat # ab110170
Lipofectamine™ RNAiMAX transfection reagent	Thermofisher Scientific	Cat # 13778150
Lipofectamine™ LTX reagent with PLUS reagent	Thermofisher Scientific	Cat # 15338030
Lipofectamine™ 2000 transfection reagent	Thermofisher Scientific	Cat # 11668019
QuikChange II XL Site-Directed Mutagenesis Kit	Agilent technologies	Cat # 200523
Experimental Models: Organisms/Strains		
C57BL/6J	Jackson Lab	stock 000664
Il1a $^{-/-}$	University of Tokyo	Dr. Yoichiro Iwakura
Atg16l1$^{fl/fl}$*LysMCre*	Cedars- Sinai Medical Center	Dr. David Shih
Oligonucleotides, plasmids and PCR primers		
pHIV-dTomato	Addgene	pHIV-dTomato was a gift from Bryan Welm (Addgene plasmid #21374; http://n2t.net/addgene:21374; RRID:Addgene_21374)
psPAX2	Addgene	psPAX2 was a gift from Didier Trono (Addgene plasmid # 12260; http://n2t.net/addgene:12260; RRID:Addgene_12260)

pMD2.G	Addgene	pMD2.G was a gift from Didier Trono (Addgene plasmid # 12259; http://n2t.net/addgene:12259; RRID:Addgene_12259)
PCR amplification primers for cloning IL-1a-Flag into pHIV-dTomato: IL-1a fwd – EcoRI: 5'-CCCGAATTCACCATGGCCAAAGTTCCTGACTTGTTTGAAGACC-3' IL-1a rev – BamHI: 5'-CCCGGATCCTTACTTATCGTCGTCATCCTTGTAATCAGAGCCTCC-3'	Invitrogen	PCR template: mouse IL-1a-Flag cDNA clone (Sino Biological Inc; MG50114-CF) Custom primers (Invitrogen)
siRNA negative control	MyBiosource	MBS8241404
IL-1A siRNA	MyBiosource	MBS8200312
HAX1 siRNA	MyBiosource	MBS8220685
PLSCR3 siRNA	MyBiosource	MBS8212879
Human IL1F1/IL1a-Flag cDNA clone	Sino Biological Inc	HG10128-CF
Mouse IL1F1/IL1a-His cDNA clone	Sino Biological Inc	MG50114-NH
Mouse IL1F1/IL1a-Flag cDNA clone	Sino Biological Inc	MG50114-CF
NLRP3 Left; 5'-TCCACAATTCTGACCCACAA-3' Right; 5'-ACCTCACAGAGGGTCACCAC-3'		http://www.ncbi.nlm.nih.gov/nuccore/NM_145827.3
IL-1a Left; 5'-AGACCATCCAACCCAGATCA-3' Right; 5'-TGACAAACTTCTGCCTGACG-3'		http://www.ncbi.nlm.nih.gov/nuccore/NM_010554.4
IL-1b Left; 5'-CAGGCAGGCAGTATCACTCA-3' Right; 5'-TGTCCTCATCCTGGAAGGTC-3'		http://www.ncbi.nlm.nih.gov/nuccore/NM_008361.3
GAPDH Left; 5'-ACCCAGAAGACTGTGGATGG-3' Right; 5'-GGATGCAGGGATGATGTTCT-3'		http://www.ncbi.nlm.nih.gov/nuccore/GU214026.1
IL-18 Left; 5'-TCCATGCTTTCTGGACTCCT-3' Right; 5'-GGCTTTCTTTGTCCTGATGC-3'		https://www.ncbi.nlm.nih.gov/nuccore/NM_008360
Software and Algorithms		
Prism 7.0	GraphPad Software	https://www.graphpad.com
Image Lab	Bio-Rad Laboratories	http://www.bio-rad.com/en-cn/product/image-lab-software

BZ-X analyzer	Keyence	https://www.keyence.com/ss/products/microscope/bz-x700/
Summit V4.3 Flow cytometry	Dako Colorado, Inc	
Leica Microsystems LAS AF Lite	Leica microsystems	
FlowJo 10.6.1	BD	
Echo Revolve Fluorescence Microscope	Echo	
Varioskan™ LUX multimode microplate reader	Thermofisher Scientific	
Other		
SuperSignal West Pico PLUS Chemiluminescent Substrate	Thermofisher Scientific	Prod # 34577
Fixation/Permeabilization Solution kit	BD Biosciences	Cat # 554714
Sea Block serum free-PBS	abcam	Cat # ab166955

Contact for Reagent and Resource Sharing

Further information and requests for resources and reagents should be directed to and will be fulfilled by Moshe Arditi (Moshe.Arditi@cshs.org).

SI References

1. K. Arnold, L. Bordoli, J. Kopp, T. Schwede, The SWISS-MODEL workspace: a web-based environment for protein structure homology modelling. *Bioinformatics* **22**, 195-201 (2006).
2. H. M. Berman *et al.*, "The Protein Data Bank, 1999" in International Tables for Crystallography Volume F: Crystallography of biological macromolecules. (Springer, 2006), pp. 675-684.
3. D. Xu, L. Jaroszewski, Z. Li, A. Godzik, AIDA: ab initio domain assembly server. *Nucleic acids research* **42**, W308-W313 (2014).
4. J. Phillips *et al.*, Scalable molecular dynamics with NAMD. *J. Comput. Chem.* **26**, 1781-1802 (2005).
5. A. D. MacKerell *et al.*, All-atom empirical potential for molecular modeling and dynamics studies of proteins. *J Phys Chem B* **102**, 3586-3616 (1998).
6. S. Miyamoto, P. A. Kollman, Settle - an Analytical Version of the Shake and Rattle Algorithm for Rigid Water Models. *J. Comput. Chem.* **13**, 952-962 (1992).
7. A. Bakan, L. M. Meireles, I. Bahar, ProDy: protein dynamics inferred from theory and experiments. *Bioinformatics* **27**, 1575-1577 (2011).
8. A. Bakan *et al.*, Evol and ProDy for bridging protein sequence evolution and structural dynamics. *Bioinformatics* **30**, 2681-2683 (2014).
9. D. Comaniciu, P. Meer, Mean shift: A robust approach toward feature space analysis. *IEEE Trans. Pattern Anal. Mach. Intell.* **24**, 603-619 (2002).
10. I. Cohen *et al.*, IL-1alpha is a DNA damage sensor linking genotoxic stress signaling to sterile inflammation and innate immunity. *Sci. Rep.* **5**, 14756 (2015).

11. S. Jo, T. Kim, V. G. Iyer, W. Im, CHARMM-GUI: a web-based graphical user interface for CHARMM. *J Comput Chem* **29**, 1859-1865 (2008).

12. S. Jo, J. B. Lim, J. B. Klauda, W. Im, CHARMM-GUI Membrane Builder for mixed bilayers and its application to yeast membranes. *Biophys J* **97**, 50-58 (2009).

13. J. Lee *et al.*, CHARMM-GUI input generator for NAMD, GROMACS, AMBER, OpenMM, and CHARMM/OpenMM simulations using the CHARMM36 additive force field. *J. Chem. Theo. Comput.* **12**, 405-413 (2015).

14. R. Apweiler *et al.*, UniProt: the universal protein knowledgebase. *Nuc. Acids Res.* **32**, D115-D119 (2004).

15. W. Humphrey, A. Dalke, K. Schulten, VMD: visual molecular dynamics. *J. Mol. Graph.* **14**, 33-38 (1996).

16. A. Bakan *et al.*, Evol and ProDy for bridging protein sequence evolution and structural dynamics. *Bioinformatics* **30**, 2681-2683 (2014).

17. M. Larkin *et al.*, Clustal W and Clustal X version 2.0. *Bioinformatics* **23**, 2947-2948 (2007).

18. A. M. Waterhouse, J. B. Procter, D. M. Martin, M. Clamp, G. J. Barton, Jalview Version 2--a multiple sequence alignment editor and analysis workbench. *Bioinformatics* **25**, 1189-1191 (2009).

Movie S1 and S2. WT (S1) and *Il1a*$^{-/-}$ (S2) peritoneal macrophages were treated with LPS and ATP and stained with TMRM to observe mitochondrial membrane potential changes.